Journal of New Technology and Materials
JNTM
Vol. 06, N°02 (2016)44-55

OEB Univ. Publish. Co.

Numerical Analysis Of Turbulent Forced-Convection Flow In A Channel With Staggered L-Shaped Baffles

Y. Menni, A. Azzi , C. Zidani and B. Benyoucef

Unit of Research on Materials and Renewable Energies - URMER -

Department of Physics, Faculty of Sciences, Abou Bekr Belkaid University,

BP 119-13000-Tlemcen, Republic of Algeria,

Corresponding author: email: czidani10@yahoo.fr

Received date: April 05, 2016; revised date: December 03, 2016; accepted date: December 11, 2016

Abstract

Characteristics of fluid flow and heat transfer are analyzed for a constant property fluid flowing turbulently through a two-dimensional horizontal rectangular cross section channel with staggered, transverse L-shaped baffles (STLBs) and a constant temperature along both walls. The Commercial CFD software FLUENT 6.3 is used to simulate the fluid flow and heat transfer fields. As a part of the same package, a preprocessor Gambit is used to generate the required mesh for the solver. The governing equations, based on the Shear Stress Transport (SST) k-ω model used to describe the turbulence phenomena, are discretized using the Finite Volume Method (FVM) with Semi Implicit Method for Pressure-Linked Equations (SIMPLE) algorithm for pressure-velocity coupling. Air is the working fluid with the flow rate in terms of Reynolds numbers ranging from 12,000 to 30,000. The effects of the baffle L-shape as well as Reynolds numbers are examined. A detailed description of turbulent heat transfer flow behaviors around the STLBs was presented. In particular, contour plots of velocity and pressure fields, axial velocity profiles, local and average heat transfer coefficients, and friction loss evaluations were obtained at constant wall temperature condition along the top and bottom channel walls. The numerical results are validated with available rectangular-baffle measured data and found to agree well with measurement. The results reveal essentially, that the flow pattern of using STLBs is characterized by strong deformations and large recirculation regions. The highest values in the velocity and pressure fields are found near the top channel wall with an acceleration process that starts just after the second STLB. Also, an increase in the Reynolds number causes a substantial increase in the Nusselt number but the pressure loss is also very significant.

Keywords: CFD ; Finite volume method ; Forced-convection ; L-shaped baffle ; Rectangular channel ; Turbulent flow.

1. Introduction

The use of baffles and fins in channels is commonly used for passive heat transfer enhancement strategy in single phase internal flow. Considering the rapid increase in energy demand, effective heat transfer enhancement techniques have become important task worldwide. Some of the applications of passive heat transfer enhancement strategies are in process industries, thermal regenerator, Shell-and-tube type heat exchanger, Internal cooling system of gas turbine blades, radiators for space vehicles and automobiles, etc. In literature, numerous studies on baffled channel heat transfer are reported, but only the relevant articles are cited here. Yuan [1] reported a numerical study for the characteristics of the periodically fully developed turbulent flow and heat transfer in a channel with transverse opposite-positioned fins. The influence of the thermal boundary condition of the fin to the heat transfer was verified. Yuan and others also studied experimentally the duct with periodic rectangular fins along the main flow direction [2] and the duct with winglet fins [3]. They can both increase heat transfer largely comparing with smooth duct. An experimental investigation was done by Habib et al. [4] to study the characteristics of the turbulent flow and heat transfer inside the periodic cell formed between segmented baffles staggered in a rectangular duct. The parameters of the experimental work were the Reynolds number and the baffle height. The results indicated that the pressure loss increases as the baffle height does, for a given flow rate. Also, the local and average heat transfer parameters increase with increasing Reynolds number and baffle height. Demartini et al. [5] presented the numeric and experimental analysis of the turbulent flow of air inside a channel of rectangular section, containing two rectangular baffle plates. Hot wire anemometry and the Finite Volume Method, by means of commercial program FLUENT 5.2 were applied in that research work. Tsay et al. [6] numerically investigated the heat transfer enhancement due to a vertical baffle in a backward-facing step flow channel. The effect of the baffle height, thickness and the distance between the baffle and the backward facing step on the flow structure was studied in detail for a range of Reynolds number varying from 100 to 500. They found that an introduction of a baffle into the flow could increase

the average Nusselt number by 190%. They also observed that the flow conditions and heat transfer characteristics are strong function of the baffle position. The heat transfer enhancement in a heat exchanger tube by installing a baffle was reported by Nasiruddin and Kamran Siddiqui [7]. In that study, the effect of baffle size and orientation on the heat transfer enhancement was studied in detail. The results showed that a significant heat transfer enhancement in a heat exchanger tube can be achieved by introducing a baffle inclined towards the downstream side, with the minimum pressure loss. Numerical studies for both solid and porous baffles in a two dimensional channel for the turbulent flow [8] and for the laminar flow regimes [9,10] were conducted and similar thermal performance results for both the solid and porous cases were reported. Ko and Anand [11] carried out an experiment for turbulent channel flow with porous baffles and found that the porous baffles present a flow behavior as good as the one with solid baffles. Dutta and Dutta [12] first reported the enhancement of heat transfer with inclined solid and perforated baffles. In that study, the effects of baffle size, position, and orientation were studied for internal cooling heat transfer augmentation. Dutta and Hossain [13] experimentally investigated the local heat transfer characteristics and the associated frictional head loss in a rectangular channel with inclined solid and perforated baffles. A combination of two baffles of same overall size was used in their experiment. The upstream baffle is attached to the top heated surface, while the position, orientation, and the shape of the other baffle are varied to identify the optimum configuration for enhanced heat transfer. A constant surface heat flux was applied from the top surface, but the bottom and the side surfaces were maintained at an adiabatic condition. The experimental results showed that the local Nusselt number distribution is strongly depended on the position, orientation, and geometry of the second baffle plate. The friction factor ratio goes up with an increase in the Reynolds number, but its value depends on the arrangement of baffles. Karwa and Maheshwari [14] presented results of an experimental study of heat transfer and friction in a rectangular section duct with fully perforated baffles (open area ratio of 46.8%) or half perforated baffles (open area ratio of 26%) at relative roughness pitch of 7.2-28.8 affixed to one of the broader walls. The authors showed an enhancement of 79-169% in Nusselt number over the smooth duct for the fully perforated baffles and 133-274% for the half perforated baffles while the friction factor for the fully perforated baffles is 2.98-8.02 times of that for the smooth duct and is 4.42-17.5 times for the half perforated baffles. Later on, a number of research groups have utilized the perforated baffle concept for internal cooling augmentation both experimentally [15] and numerically [16-18]. In those studies, different aspect ratio channels and different porosity baffles were used. Other authors studied in detail the effect of the shape of baffles and orientations on the heat transfer enhancement in the heat exchanger channels. Laminar periodic flow and heat transfer in a two dimensional horizontal channel with isothermal walls and with staggered diamond-shaped baffles was investigated numerically by Sripattanapipat and Promvonge [19]. Wang et al. [20] summarized computational and experimental results for research on the flow and heat transfer process of a rectangular channel embedded with staggered pin fins of various shapes (i.e., circular, elliptical, and drop-shaped) in a staggered arrangement. Guerroudj and Kahalerras [21] reported a numerical simulation of laminar mixed convective in a two-dimensional parallel plate channel provided with porous blocks of various shapes (i.e., rectangular, trapezoidal, and triangular-shaped). Benzenine et al. [22] presented a computational analysis of the turbulent flow of air in a pipe of rectangular section provided with two waved fins sequentially arranged in the top and the bottom of the channel wall. The influence of baffle turbulators on heat transfer augmentation in a rectangular channel with Z-shaped baffles was investigated experimentally and numerically by Sriromreun et al. [23]. Numerical and experimental predictions of the flow and heat transfer in shell-and-tube heat exchangers helical baffles were investigated by Lei et al. [24], Dong et al. [25], and Wen et al. [26]. Other similar works can be found in literature as Promvonge [27,28], Promvonge and Kwankaomeng [29], Tamna et al. [30], and Jedsadaratanachai et al. [31] studied the heat transfer and flow over V-shaped baffles submitted to laminar and turbulent flows using numerical and experimental techniques. All these shapes increase thethermal transfer rate but created catastrophic pressure losses.The principal objective of the present study is to show the influence of STLBs on the fluid flow and heat transfer characteristics when the Reynolds number effects are simultaneously present. This was decided after literature search has revealed that no work has been reported on the computation of the flow in L-baffled rectangular channels. This has motivated the present numerical simulation which is a contribution to the previous studies on improvement techniques of heat transfer. Throughout the study, a constant temperature is assumed from the entire wall of the computational domain. The simulation results of an L-shaped obstacle pair are also compared with conventional CFD simulations and the experimental data of previous researchers.

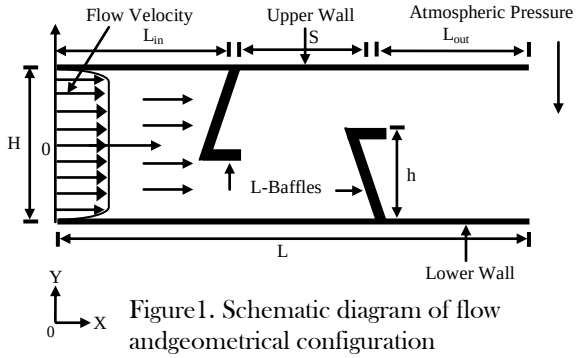

Figure1. Schematic diagram of flow andgeometrical configuration

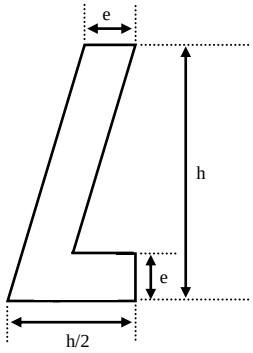

Figure 2. Cross-sectional geometry of the L-shaped baffle

2. Physical model

The system of interest is a two-dimensional isothermal wall rectangular cross section channel with a staggered transverse L-shaped baffle pair placed on both the upper and lower walls in staggered arrangement and pointing towards the upstream end as shown in Figure 1. A schematic view of the baffle shape is shown in Figure 2. The flow is two-dimensional, turbulent, incompressible and in steady state with no internal heat generation and neglecting viscous dissipation. The Prandtl number is taken equal to 0.71. All physical properties of the fluid and solid are considered to be constant.

The geometric dimensions of our problem have been based on the experimental work of Demartini et al. [5]. In their study, the experiment was conducted in a two-dimensional domain, which represents a rectangular duct of L = 0.554 m long and H = 0.146 m high, provided by two baffle plates, through which a steady flow of turbulent air. The first plate is attached to the top wall at a distance of Lin = 0.218 m and the second inserted to the bottom wall at Lout = 0.37 m from the entrance. The distance between the upper edge of the baffle and the wall was kept constant at h = 0.08m. This corresponds to the area reduction of 54.794 % at the baffle edge. The thickness of the two baffles is a e = 0.01 m.

3. Mathematical modeling

Based on the above assumptions, the channel flow is governed by continuity,Navier-Stokes and energy equations, respectively

$$\nabla\vec{V} = 0 \tag{1}$$

$$\rho\left(\vec{V}.\nabla\vec{V}\right) = -\nabla P + \mu_f \nabla^2 \vec{V} \tag{2}$$

$$\rho C_p \left(\vec{V}.\nabla T\right) = K_f \nabla^2 T \tag{3}$$

where: $\vec{V}$ is the velocity vector. Prepresents the pressure. ρ, μ, K and $C_p$are the density, the dynamics viscosity, the thermal conductivity and specific heat of fluid, respectively.

To ensure realistic accurate turbulent modeling, the performance of four different turbulent models, namely Spalart-Allamaras model, Standard k-ε model, Shear Stress Transport (SST) k-ωmodel, and Reynolds Stress model were evaluated by Nasiruddin and Kamran Siddiqui [7], solving Navier-Stokes equations. The comparison of the simulated results obtained from these turbulent models with the experimental data made the selection easy. In that study, the SST k-ωmodel was found to be the one that most accurately predicts the flow and modification due to the baffle. The selected turbulent model is capable of calculating the rapidly evolving two-dimensional flow and also in predicting, interactions with the wall. Another advantage of the selected turbulent model is that the model equations behave appropriately in both the near-wall and far-field regions. The SST k-ωmodel is defined by two transport equations, one for the turbulent kinetic energy, k and the other for the specific dissipation rate ω, as given below [32]

$$\frac{\partial}{\partial x_i}(\rho k u_i) = \frac{\partial}{\partial x_j}\left(\Gamma_k \frac{\partial k}{\partial x_j}\right) + G_k - Y_k + S_k \tag{4}$$

$$\frac{\partial}{\partial x_i}(\rho \omega u_i) = \frac{\partial}{\partial x_j}\left(\Gamma_\omega \frac{\partial \omega}{\partial x_j}\right) + G_\omega - Y_\omega + D_\omega + S_\omega \tag{5}$$

Where

$$G_k = -\rho\overline{u_i' u_j'}\frac{\partial u_j}{\partial x_i} \tag{6}$$

$$G_\omega = \alpha\frac{\omega}{k}G_k \tag{7}$$

$$\Gamma_k = \mu + \frac{\mu_t}{\sigma_k} \tag{8}$$

and

$$\Gamma_\omega = \mu + \frac{\mu_t}{\sigma_\omega} \tag{9}$$

In these equations, x_i and $x_j$are the spatial coordinates. G_k represents the generation of turbulence kinetic energy due to mean velocity gradients. $G_\omega$represents the generation of ω. Γ_k and $\Gamma_\omega$represent the effective diffusivity of k and ω, respectively. Y_k and $Y_\omega$represent the dissipation of k and ω due to turbulence, respectively. D_ω represents the cross-diffusion term. S_k and $S_\omega$are user-defined source terms.

The commercial CFD software FLUENT6.3 [33] is used to calculate the heat and fluid flow characteristics in the computational domain with STLBs. The governing equations were discretized by the QUICK-scheme [34],

decoupling with the SIMPLE-algorithm [34] and solved using the Finite Volume Method [34]. For closure of the equations, the SST k-ω model [32] was used in the present study. The mesh was generated by the pre-processor software Gambit 2.3.Structured meshes, with type-Quadrilateral elements were built and tested with the Fluent 6.3 [33]. To ensure the independence of the mesh with the numerical results, a serial of test was performed. To control the update of the computed variables for all iterations, under relaxation was varied between 0.3 and 1.0. The solutions were converged when the normalized residual values were less than 10^{-7} for all variables but less than 10^{-9} only for the energy equation.

3.1 Boundary conditions

The The hydrodynamic boundary conditions are chosen according to the experimental work of Demartini et al. [5] while the thermal boundary conditions are set according to the numerical work of Nasiruddin and Kamran Siddiqui [7]. Air was used as the working fluid for all simulation runs. The boundary conditions were given as, (i) the air entered the channel at ambient temperature with a uniform one-dimensional velocity ($u = U_{in}$, $v = 0$, $T_{in} = 300$ K); (ii) the pressure at the inlet of the computational domain was set equal to the zero (gauge); (iii) the turbulence intensity was kept at $I = 2$ % at the inlet; (iv) A constant temperature of 102°C ($T_w = 375$ K) was applied on the entire wall of the computational domain as the thermal boundary condition. (v) impermeable boundary and no-slip wall conditions are imposed at the walls; and (vi) in the channel outlet it is prescribed the atmospheric pressure ($P = P_{atm}$). The Reynolds number of the experiments [5] is Re $= 8.73\times10^4$, defined as

$$\mathrm{Re} = \frac{\rho \overline{U} D_h}{\mu} \tag{10}$$

where $\overline{U}$ is the entrance (reference) velocity, 7.8 m/s, and D_h is the hydraulic diameter of the channel, equal to 0.167 m. The total length of the channel is equivalent to 3.307 × D_h, which is not sufficient for the flow development. Therefore,no influence will result from the side walls, so that the flow can be considered as being two-dimensional.

The skin friction coefficient, Cf, is given by

$$Cf = \frac{\tau_w}{\frac{1}{2}\rho \overline{U}^2} \tag{12}$$

The numerical friction factor was computed from the pressure drop, ΔP, across the length of computational flow domain, L, having the hydraulic diameter, using Darcy Weisbach formula. That is,

$$f = \frac{(\Delta P/L) D_h}{\frac{1}{2}\rho \overline{U}^2} \tag{13}$$

The local Nusselt number, Nu_x is evaluated as follows

$$Nu_x = \frac{h_x D_h}{\lambda_f} \tag{14}$$

The average Nusselt number, Nu_{av} can be obtained by

$$Nu_{av} = \frac{1}{L}\int Nu_x \partial x \tag{15}$$

where h_x represents the local convective heat transfer coefficient

3.2 Grid sensitivity

The mesh was generated by the Pre-processor software Gambit 2.3. The mesh was refined at all solid boundaries, with volumes growing in geometrical progression with the increasing distance from the wall, as given by the expression

$$a_n = a_1\left(q^{n-1}\right) \tag{16}$$

where a_n is the length of the last volume from the wall, a_1 is the length of the first volume adjacent to the wall, q is the growth ratio and n is the number of volumes. This expression is valid for the regions near the walls. For the regions more distant from the walls, the mesh is uniform, as reported by Demartini et al. [5]. A fine non-uniform mesh with the minimum cell number of (220 × 95) and the maximum cell number of (420 × 235) were provided through the walls. It is found that the variation in Nu_{av} and f values for the staggered L-shaped baffles at $Pi = 0.142$ and Re $= 8.73 \times 10^4$ is marginal when increasing the number of cells from (220 × 95) to (420 × 235). Hence, there is no such advantage in increasing the number of cells beyond this value. Considering both convergent time and solution precision, the grid system of (220 × 95) cells (in X and Y directions, respectively) was adopted for the current computation. The grid density was kept higher in the vicinity of the heated wall and the STLBs to capture the variations in the flow and temperature fields within the hydraulic and thermal boundary layers.

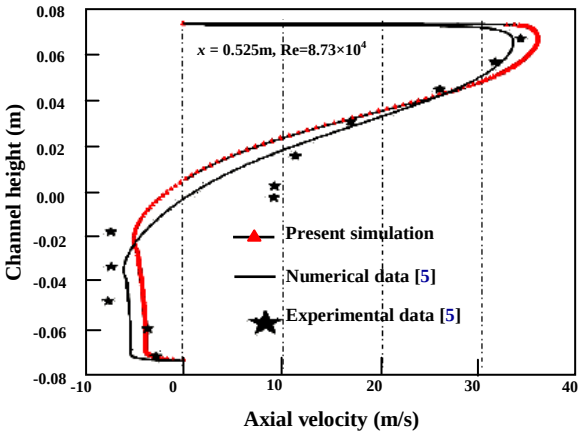

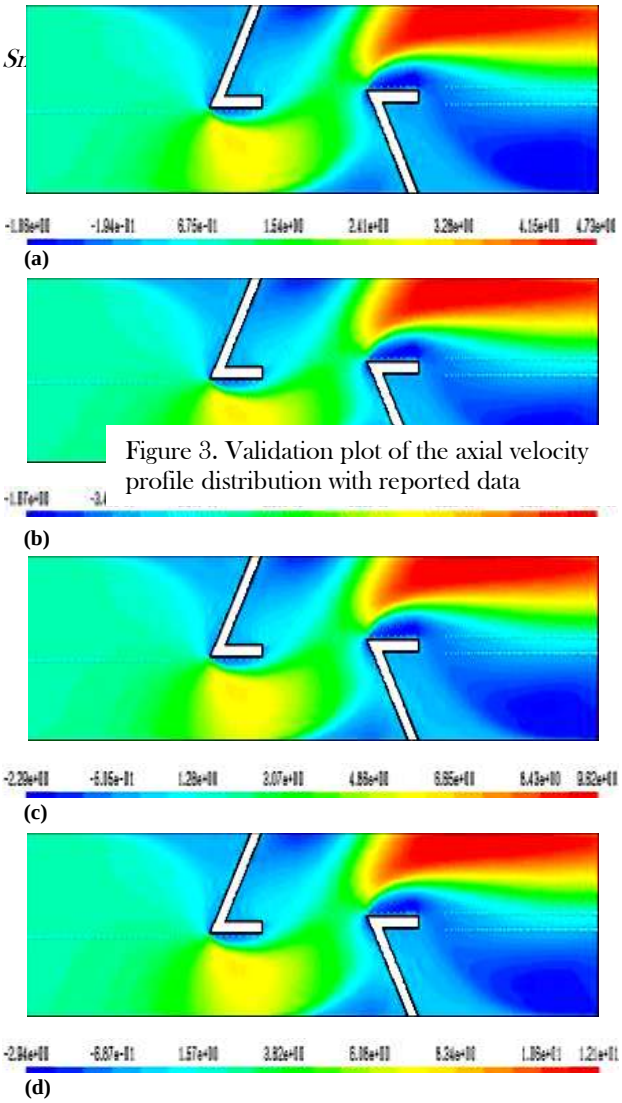

Figure 4. Two-dimensional axial velocity field in the L-baffled channel at different flowReynolds numbers: (a) Re = 12,000, (b) Re = 18,000, (c) Re = 24,000, and (d) Re = 30,000. Airflow is from left to right. Velocity values in m/s.

4. Results and discussion

To verify our numerical simulation, a comparizon was made with the numerical and experimental data obtained by Demartini et al. [5] in the case of a rectangular channel, where two baffle plates were placed in opposite walls. The geometry of the problem is a simplification of the geometry of baffle plates found in shell-and-tube heat exchangers.

A quantitative comparison between both the experimental and numerical velocity profiles after the lower wall baffle, near the channel outlet is shown in Figure 3. For the case of axial velocity profiles at a position x = 0.525 m, measured downstream of the entrance, there is a good agreement between the present study and previous work [5]. These results give confidence that the numerical scheme used was accurate.

The two-dimensional horizontal constant temperature-surfaced rectangular cross section channel flow structure in the presence of STLBs could be easily discerned by considering the velocity contour plots in Figure 4(a-d). The figures present axial velocity fields of turbulent channel flow through STLBs using the SST k-ω model for Re = 12,000, 18,000, 24,000, and 30,000, respectively. The largest variations in the velocity fields occur in the regions near to the staggered STLBs, as expected. The peak velocity values are seen near the heated top channel wall with an acceleration process that starts just after the lower wall STLB, while the velocity is observed to be very low at the locations corresponding to the zones of counter rotating flow in the regions downstream of both STLBs as seen in the figure. In the regions between the tip of both STLBs and the channel walls, the velocity is increased. The effect of the flow rate on the fluid velocity is also depicted in the figure which shows that the velocity value increases with the increase of Reynolds number.

The structure of the near wall flow in the channel with two solid STLBs which are arranged on the top and bottom channel walls in a periodically staggered way can be displayed by considering the axial velocity profile plots in transverse stations for four different Reynolds number values (Re = 12,000, 18,000, 24,000, and 30,000) as depicted in Figure 5(a-g) at various axial positions, x = 0.159, 0.189, 0.255, 0.285, 0.315, 0.345, and 0.525 m, respectively. At Reynolds numbers of 12,000 to 30,000, the air flows under, between and above the STLBs by taking their exact shape with presence of recirculation zones downstream from each STLB whose size increases by increasing the Reynolds number from 12,000 to 30,000. When the inertia effects become important, the great quantity of the fluid, at a higher velocity, flows over the STLBs which will certainly causes a higher heat transfer than that of the lower Reynolds number. Between and downstream the STLBs there is appearance of larger vortices whose size changes with the value of the Reynolds number. The comparison of axial velocity profiles at different axial stations shows that the influence of the deformation of the flow field increases as the air approaches the upper wall STLB, increasing the velocity of the flow approaching the passage under the baffle (see x = 0.159 m and x = 0.189 m in the figure). The plots also show that as the flow is accelerated and redirected near the first STLB, a very small recirculation zone is formed in the vicinity of the upper left corner (see Fig. 5a and b). Downstream of the first STLB, as a result of sudden expansion in the cross-section, the airflow separates, a larger clockwise vortex is formed behind the upper wall STLBs in the upper part of the channel andflow reattachment is then established (see Fig. 5c and d).

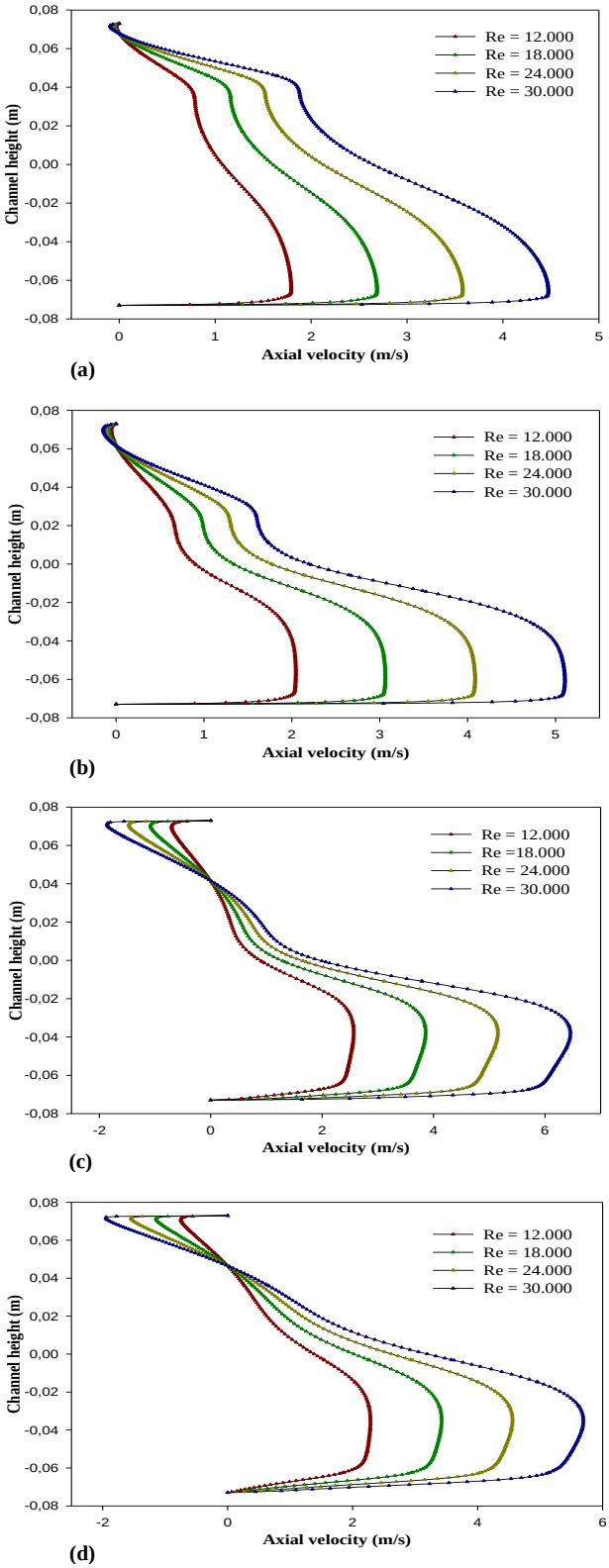

Figure 5.Plots of axial velocity profiles at axial stations given by (a) x=0.159 m, (b) x=0.189 m, (c) x=0.255m, (d) x=0.285 m, (e) x= 0.315 m, (f) x=0.345 m, and (g) x=0.525 m, measured downstream of the entrance

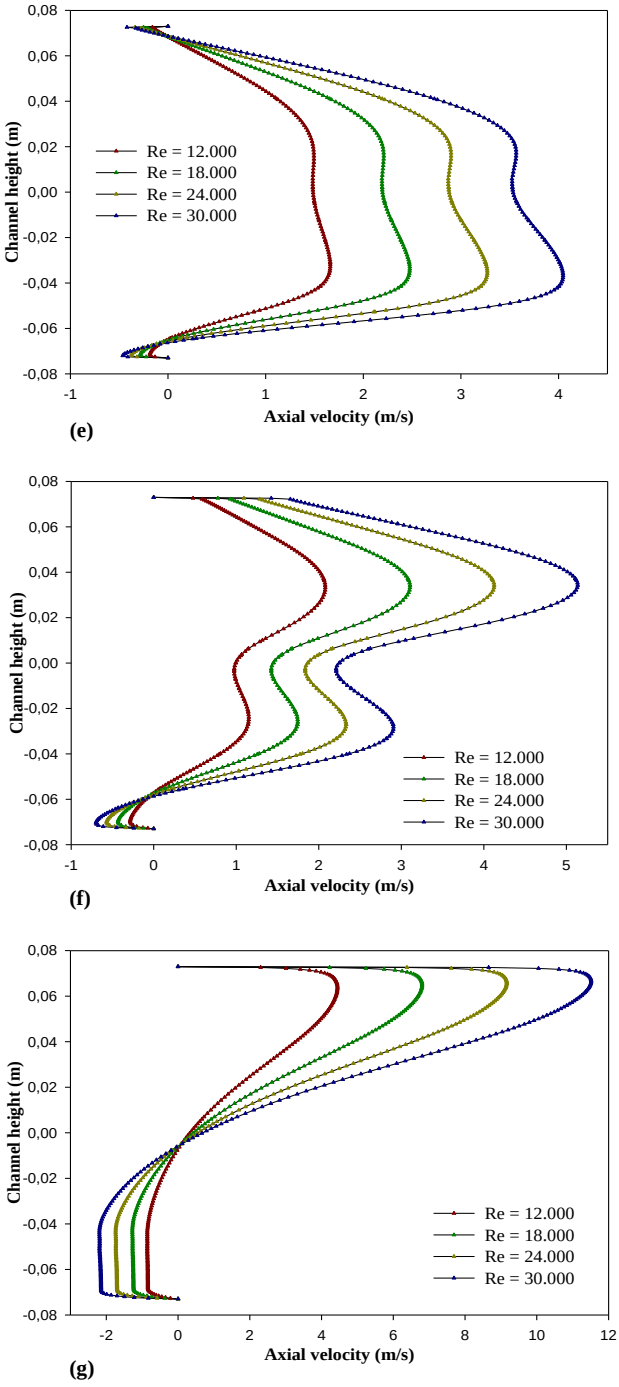

Figure 5. (Continued)

In the region opposite the first STLB, the flow is characterized by very high velocities, approaching 237.7% of the inlet velocity, which is 1.049m/s at the lowest value of Re number, as shown in Fig. 5(c and d). A similar behavior is observed near the STLB mounted on the lower wall with counterclockwise vortices at the upstream (see Fig. 5e and f) and downstream STLB (see Fig. 5g). The plots if Figure 5(e and f) shows that as the airflow

approaches the second STLB, its velocity is reduced in the lower part of the channel, while in the upper part is increased. In these locations (x = 0.315 m and x = 0.345 m) the negative velocities indicate the presence of a small recirculation zone at the lower left corner behind the lower wall STLB. The axial velocity profile distribution obtained for different values of Reynolds number after the lower wall STLB, near the channel outlet is also shown in Figure 5. At a position x = 0.525 m, 0.145 m after the second STLB and 0.029 m before channel outlet, the value of the velocity reaches 4.443m/s, 4.233 times higher than the entrance velocity at the lowest value of Re number, as shown in Figure 5g. In the lower part of the channel, a strong counterclockwise vortex is observed downstream of the considered baffle, which was induced due to the flow separation. The vortex is located close to the solid wall and its height was approximately equal to the extent of the flow blockage by the STLB, which is equal to 0.08m (see Fig. 5g).

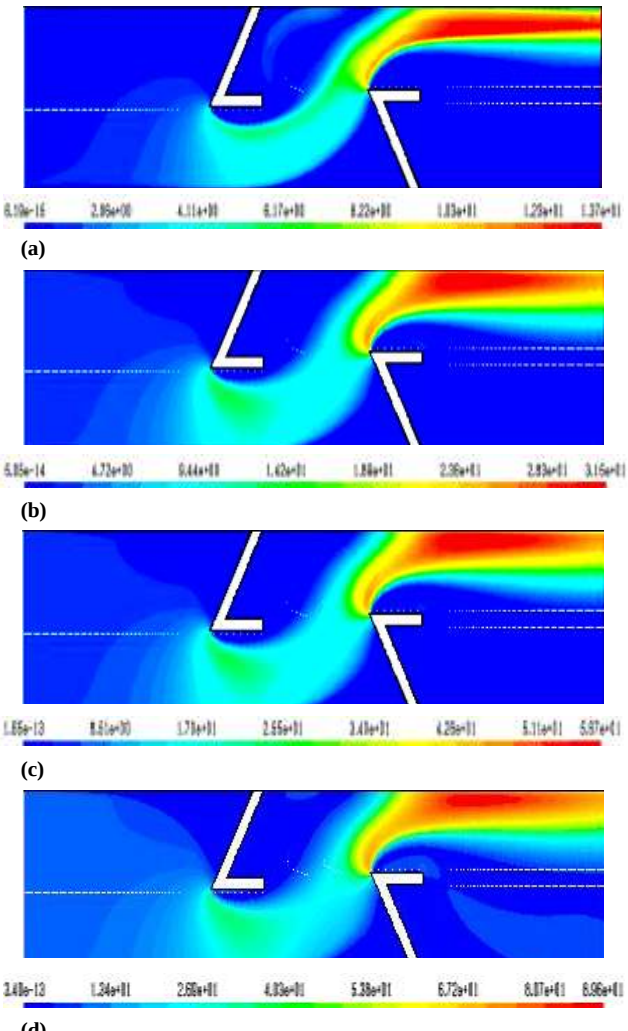

Figure 6. Two-dimensional dynamic pressure field in the L-baffled channel at different Reynolds numbers: (a) Re = 12,000, (b) Re = 18,000, (c) Re = 24,000, and (d) Re = 30,000. Airflow is from left to right. Dynamic pressure values in Pa.

The presence of the STLBs influences not only the velocity field but also the pressure distribution in the whole domain examined. The contour plots of dynamic pressure are shown in Figure 6 (a-d) for different Re values. The plots in Figure 6 show very low dynamic pressure values adjacent to the STLBs. In the regions downstream of both STLBs, recirculation cells with very low dynamic pressure values are observed. This fact is associated to the negative velocities at the upstream and downstream both STLBs shown in Figure 5. In the regions between the tip of the STLBs and the channel walls, the dynamic pressure is increased.

It indicates that the highest dynamic pressure value can be observed at the area of high velocities especially at the area near the upper channel wall with an acceleration process that starts just after the second STLB.

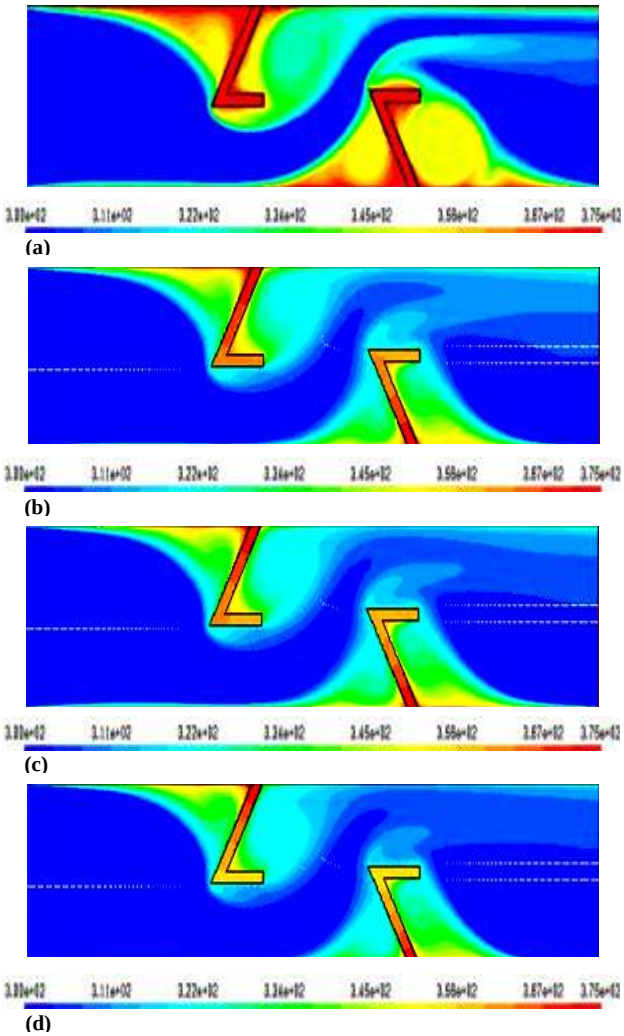

Figure 7. Two-dimensional temperature field in the L-baffled channel at different Reynolds numbers: (a) Re = 12,000, (b) Re = 18,000, (c) Re = 24,000, and (d) Re =

30,000. Airflow is from left to right. Fluid temperature values in K.

The temperature field is an important indicator to reflect the performance of a baffled channel. The contour plots of temperature field distributions in the given channel with the guidance of two-STLBs and a constant wall temperature condition along the top and bottom walls for the tested Reynolds number range of 12,000-30,000 are shown in Figure 7(a-d), respectively. In the figure, the lowest temperature value can be observed where the flow impinges the channel wall, especially in the region opposite the STLB tip where the velocity in this region is somewhat high while the highest one is found at the STLB corner area where the corner recirculation zone occurs, especially area behind the STLBs. The figure shows that the fluid temperature in the recirculation region is significantly high as compared to that in the same region of no STLB. It is also shown that in the recirculation regions, the fluid temperature is increased by approximately 75% due to the insertion of STLBs. The most intense in the temperature field is that occurring downstream of the lower-wall STLB, responsible for the high flow velocities observed at the outlet of the channel, creating a negative velocity profile which introduces mass inside the test channel through the outlet (see Fig. 5g).

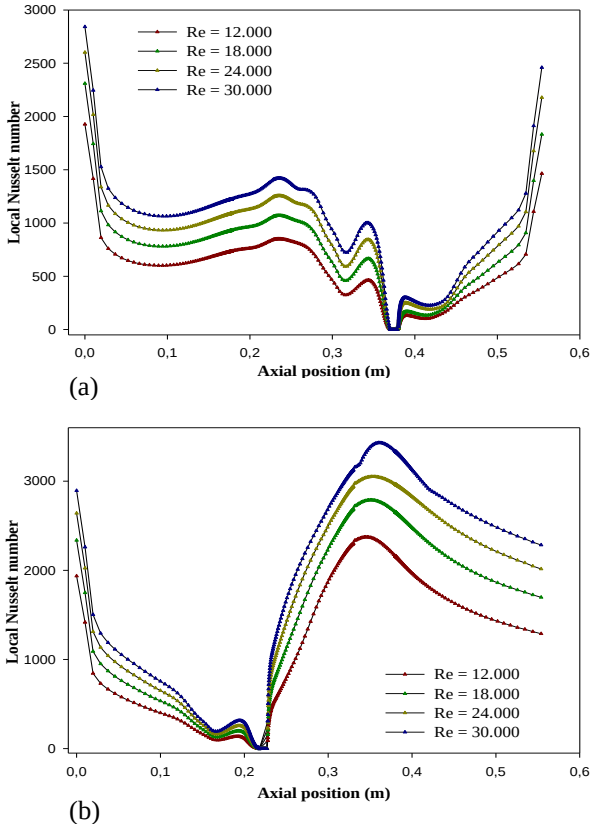

Figure 8. Axial variation of local Nusselt number with Reynolds number at the surface of (a) top and (b) bottom walls of the L-shaped baffled channel

The temperature field is also affected by the Reynolds number. Figure 7(a-d) also depicts the temperature field contour plots as a function of the Reynolds number. In the figure, it is worth noting that the fluid temperature value tends to decrease with the rise of Reynolds number for all locations due to the augmentation of the inertia forces further to the augmentation of the flow rate while the flow velocity shows an opposite trend (see Fig. 4 and 5). By increasing the Reynolds number from 12,000 to 30,000, large recirculation regions and velocity gradients are observed behind the STLBs. The generation of these vortex flows from using the STLBs as well as the role of better fluid mixing and the impingement is the main reason for the augmentation in the temperature gradient over the heating wall.

The axial distribution plots of local Nusselt number profiles as a function of Reynolds number at the surface of the lower and upper walls of the channel are shown in Figure 8(a and b), respectively. It is seen in the figure that the largest variations on both the upper and lower walls of the given channel are found near the tip of the STLBs, due to the strong velocity gradients in that region. In the regions downstream of both STLBs, the local heat transfer is significantly enhanced for all Re values investigated. This enhancement is due to the intense mixing by the vortices. Due to the changes in the flow direction produced by the STLBs, the highest Nu_x values appear in the region opposite the lower wall STLB with an acceleration process that starts just after the second STLB. Concerning the effect of the flow rate on the local heat transfer characteristics, it can see from this figure and for this range of Reynolds number ($12{,}000 \le Re \le 30{,}000$) that the Nu_x value tends to increase with the rise of Re values for all locations. This could be due to the reason that an increase in the Re value cause an increase in the length and strength of the vortices, which enhance mixing and mixing length.

The average heat transfer results are done on the heated top and bottom surfaces and presented in terms of a non-dimensional Nusselt number ration, Nu_m/Nu_0, along the tested channel walls. Nu_0 is the Nusselt number for fully developed flow in a smooth channel at the same Reynolds number, and is given by

$$Nu_0 = 0.023\,\mathrm{Re}^{0.8}\,\mathrm{Pr}^{0.4} \quad (17)$$

The Nu_0 is used as a reference to minimize the Reynolds number effect in the presented results. The Nusselt number ratio essentially indicates the amount of enhancement in heat transfer obtained by the flow guidance turbulators over the smooth rectangular channel.

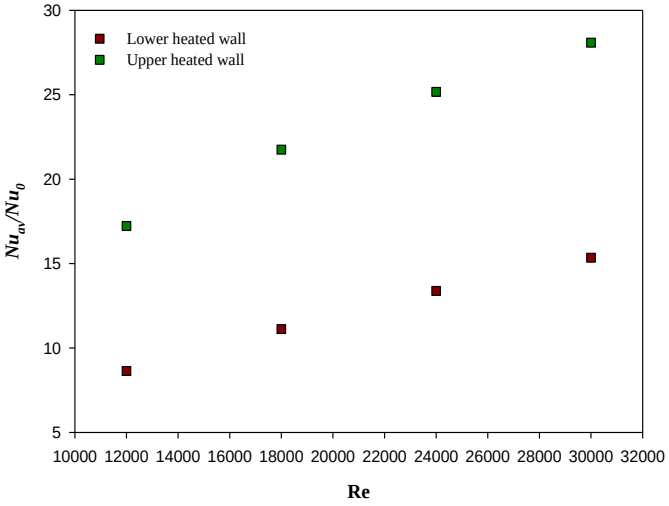

Figure 9. Variation plots of Normalized Nusselt number as a function of Reynolds number at the surface of the top and bottom channel walls

Figure 9 shows the normalized average Nusselt number versus the Reynolds number (based on the hydraulic diameter) for the channel with upper and lower wall-mounted STLBs. The figure shows as expected, that the heat transfer rate increased with the Reynolds number. Both channel walls show similar trend but with different values. The largest variations are found at the heated top surface of the channel, due to the strong velocity gradients in that region. It is also noted that the use of the STLBs lead to extremely considerable increase in the convective average Nusselt number rate in comparison with the plain channel with no baffle. The heat transfer rate value for the STLBs is found to be higher by about 8.637-28.081 times over the plain channel with no baffle, depending on the wall surface and the Reynolds number values.

Figure 10(a and b) shows the axial distribution plots of local skin friction coefficient profiles along the lower and upper channel walls in the range of Reynolds number investigated, respectively. We will start analyzing the effect of the STLB presence before discussing the influence of flow Reynolds number. Similarly to the results in Figure 8, the largest *Cf* value is found in the region opposite the upper and lower wall STLBs, due to the strong velocity gradients in that region while the smallest *Cf* value is found, firstly, upstream of the top wall STLB in the upper part of the channel and, secondly, downstream of the bottom wall STLB in the lower part of the channel, due to the orientation of the airflow by these deflectors. However, the skin friction coefficient is increased again at the locations corresponding to the zones of recirculation as seen in the figure. It indicates that the highest skin friction coefficient can be observed at the top heated surface of the channel in the area of high velocity especially at the top face of the STLB mounted on the lower wall of the channel. The variation of isothermal skin friction coefficient value with Reynolds number for the STLBs is also shown in Figure 10. It is clear from this figure that the *Cf* tends to increase with raising the Reynolds number value, as expected.

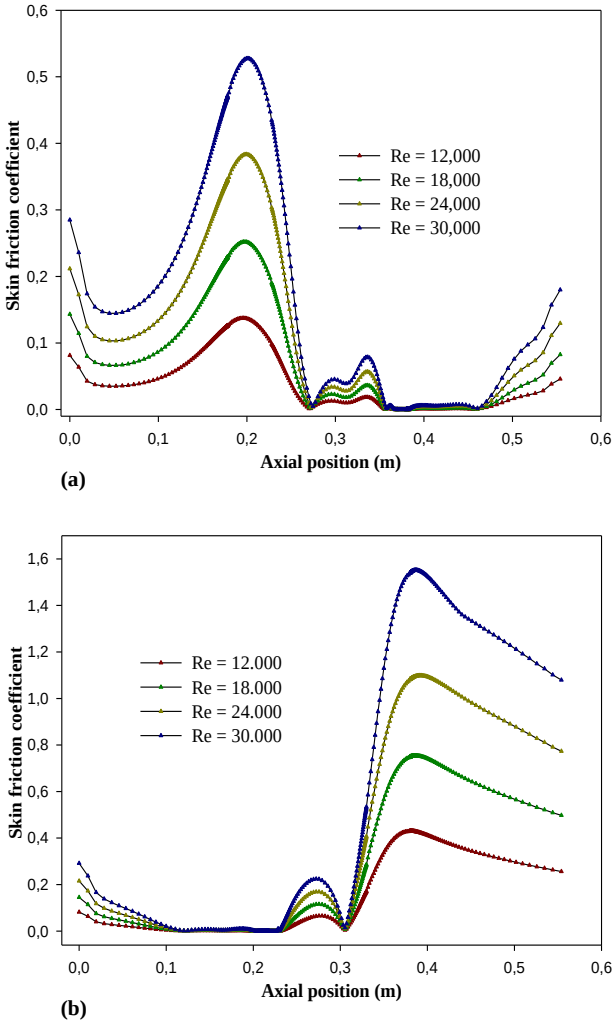

Figure 10. Axial variation of skin friction coefficient with Reynolds number at the surface of (a) top and (b) bottom walls of the L-shaped baffled channel

Figure 11 shows the variation of the dimensionless pressure drop given by the friction factor ratio, f/f_0, with Reynolds number ($12{,}000 \le Re \le 30{,}000$). Here f_0 is the friction factor in a fully developed smooth channel at the same Reynolds number, and it can be presented as

$$f_0 = \frac{1}{(0.79 \ln Re - 1.64)^2} \qquad (18)$$

As expected, obviously it can be observed that values of f/f_0 become higher with increasing values in Reynolds number.

Inthe figure, the L-shaped baffled channel flows give higher values of friction factor than that for smooth channel flow due to the induction of high recirculation or vortex flow and thin boundary layer in the baffled channel, leading to higher temperature gradients, heat transfer and pressure drop.

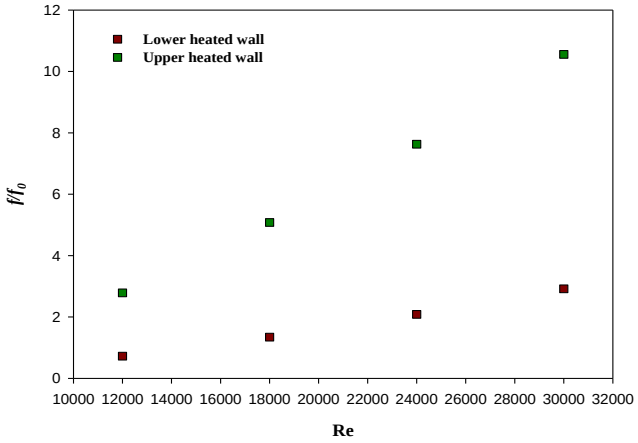

Figure 11. Normalized friction factor versus the Reynolds number at the surface of the top and bottom channel walls

The maximum f/f_0 values for both upper and lower channel walls are found to be about 0.722-2.918 and 2.784-10.554 times above those for the smooth duct with no baffle, respectively, depending on the Re values. Thus the flow blockage due to the existence of baffle as well as the role of turbulence degree in the core region is a key factor to cause an extreme pressure drop.

4. Conclusion

A numerical study has been conducted to examine the fluid flow and heat transfer characteristics in a two-dimensional horizontal constant temperature-surfaced rectangular cross section channel with lower and upper wall-mounted L-shaped baffles in the turbulent regime from Re = 12,000 to 30,000. The aim at using the STLBs is to create vortex flows having a significant influence on the flow pattern leading to higher heat transfer enhancement in the given channel. The computations are based on the Finite Volume Method, and the SIMPLE-algorithm has been implemented. The effects of the baffle L-shape geometry as well as Reynolds numbers are examined. The obtained results are compared with available experimental data from the literature and good agreement is obtained. The velocity profiles, and pressure and temperature fields over the baffled channel are the most notable characteristics of the effects of the STLB on the mainstream flow. These effects are: mainstream flow separation, recirculation, and secondary flow. The comparison of axial velocity profiles at different Reynolds numbers shows that as the airflow is accelerated and redirected near the STLBs, a very small recirculation zone is formed in the vicinity of the upper left corner. Downstream, as a result of sudden expansion in the cross-section, the flow separates, a larger clockwise recirculation zone is formed behind the upper wall STLB and flow reattachment is then established. A similar phenomenon is found near the STLB mounted on the lower wall with counterclockwise recirculation zones at the upstream and downstream STLB. The length of theses recirculation zones strongly depend on the flow Reynolds number value. The appearance of these recirculation flows can help to increase higher the heat transfer in the channel with two- STLBs because of transporting the fluid from the core to the near wall regimes, and in general, an increase in the flow Reynolds number causes a substantial increase in the flow velocity, leading to a high temperature gradient along the heating channel walls but the pressure loss is also very significant.

The above results suggest that a significant heat transfer enhancement in a heated channel can be achieved by introducing STLBs into the flow. The study can be extended for different number, sizes, positions, arrangements, orientations, and inclination angles, of the L-shaped baffles at different boundary conditions for temperature and velocity.

AUTHOR'S CONTRIBUTIONS

Each author of this manuscript made considerable contributions in developing the mathematical modeling, data-analysis and contributed to the writing of this manuscript.

NOMENCLATURE

a_n	Length of the last volume from the wall, m
a_1	Length of the first volume adjacent to the wall
Cp	Specific heat at constant pressure, J/kg K
Cf	Skin friction coefficient
D_h	Hydraulic diameter of rectangular channel, m
e	L-shaped baffle thickness, m
f	Friction factor
f_0	Friction factor in smooth channel at the same Reynolds number
G_k	Turbulent kinetic energy generation due to mean velocity gradient
G_ω	Kinetic energy generation due to buoyancy
H	Channel height, m
h	L-shaped baffle height, m
h_x	Local convective heat transfer coefficient, W/m^2K
k	Turbulent kinetic energy, m^2/s^2
L	Length of rectangular channel in x-direction, m
L_{in}	Distance upstream of the first L-shaped baffle, m
L_{out}	Distance downstream of the second L-shaped baffle, m
n	Number of volumes.

Nu_{av}	Average Nusselt number
Nu_x	Local Nusselt number
Nu_0	Nusselt number for fully developed pipe flow at the same Reynolds number
P	Pressure, Pa
P_{atm}	Atmospheric pressure, Pa
Pr	Prandtl number
q	Growth ratio
Re	Reynolds number based on the channel hydraulic diameter
S	L-shaped baffle distance or spacing, m
S_k, S_ω	Source term of k and ω
T	Temperature, °C
T_{in}	Inlet fluid temperature, °C
T_w	Wall temperature, °C
$\overline{U}$	Mean axial velocity of the section, m/s
U_{in}	Inlet velocity, m/s
u, v	Velocity component in x- and y- direction, m/s
u	Velocity component in x-direction, m/s
$\vec{V}$	Velocity vector, m/s
x, y	Cartesian coordinates, m
Y_k, Y_ω	Dissipation of k and ω

Greek symbols

ω	Specific dissipation rate, m^2/s
Γ_k, Γ_ω	Effective diffusivity of k and ω
ρ	Fluid density, kg/m^3
μ	Dynamic viscosity, Kg/m s
μ_f	Fluid dynamic viscosity, Kg/m s
μ_t	Turbulent viscosity, Kg/m s
τ_w	Wall shear stress, Kg/s^2 m
λ_f	Fluid thermal conductivity, W/m °C
ΔP	Pressure drop, Pa

Subscript

atm	Atmospheric
f	Fluid
i, j	Refers coordinate direction vectors
in, out	Inlet, outlet of the computational domain
t	turbulent
w	Wall
x	Local

6. REFERENCES

[1] Z. X. Yuan, Numerical Study of Periodically Turbulent Flow and Heat Transfer in a Channel with Transverse Fin Arrays, *Int. J. Numerical Methods for Heat & Fluid Flow*, vol. 10, N°8, pp. 842-861, (2000).

[2] Z. X. Yuan, Q. W. Wang and W. Q. Tao, Experimental Study of Enhanced Heat Transfer in Ducts with Periodic Rectangular Fins Along the Main Flow Direction, *Pro. 11th IHTC*, 23-28 August, Kyongju, Korea, vol. 5, pp. 327-32, (1998).

[3] Z. X. Yuan, W. Q. Tao and Q. W. Wang, Experimental Investigation of Heat Transfer Enhancement in Ducts with Winglet Fins, *Pro. First Int. Conference of Engineering Thermophysics*, 21-23 August, Beijing, China, pp. 457-63, (1999).

[4] M. A. Habib, A. M. Mobarak, M. A. Sallak, E. A. Abdel Hadi and R. I. Affify, Experimental Investigation of Heat Transfer and Flow over Baffles of Different Heights, *Trans. ASME J. Heat Transfer*, vol. 116, pp. 363-368, (1994).

[5] L. C. Demartini, H. A. Vielmo and S. V. Möller, Numeric and Experimental Analysis of the Turbulent Flow through a Channel with Baffle Plates, *J. the Braz. Soc. of Mech. Sci. & Eng.*, vol. 26, N° 2, pp. 153-159, (2004).

[6] Y. -L. Tsay, T. S. Chang and J. C. Cheng, Heat Transfer Enhancement of Backward-facing Step Flow in a Channel by Using Baffle Installation on the Channel Wall, *Acta Mech.*, vol. 174, N° 1-2, pp. 63-76, (2005).

[7] Nasiruddin and M. H. Kamran Siddiqui, Heat Transfer Augmentation in a Heat Exchanger Tube Using a Baffle, *Int. J. Heat and Fluid Flow*, vol. 28, pp. 318-328, (2006).

[8] Y. T. Yang, C. Z. Hwang, Calculation of Turbulent Flow and Heat Transfer in a Porous Baffled Channel, *Int. J. Heat Mass Transfer*, vol. 46, pp. 771-780, (2003).

[9] B. M. Da Silva Miranda and N. K. Anand, Convective Heat Transfer in a Channel with Porous Baffles, *Numer. Heat Transf.*, A Appl., vol 46, N° 5, pp. 425-452, (2004).

[10] N. B. Santos and M. J. S. De Lemos, Flow and Heat Transfer in a Parallel-plate Channel with Porous and Solid Baffles, *Numer. Heat Transf.*, A Appl., vol. 49, N° 5, pp. 471-494, (2006).

[11] K. H. Ko and N. K. Anand, Use of Porous Baffles to Enhance Heat Transfer in a Rectangular Channel, *Int. J. Heat Mass Transfer,* vol. 46, pp. 4191-4199, (2003).

[12] P. Dutta and S. Dutta, Effect of Baffle Size, Perforation and Orientation on Internal Heat Transfer Enhancement, *Int. J. Heat Mass Transfer*, vol. 41, N° 19, pp. 3005-3013, (1998).

[13] P. Dutta and A. Hossain, Internal Cooling Augmentation in Rectangular Channel Using two Inclined Baffles, *Int. J. Heat and Fluid Flow*, vol. 26, pp.223-232, (2005).

[14] R. Karwa and B. K. Maheshwari, Heat Transfer and Friction in an Asymmetrically Heated Rectangular Duct with Half and Fully Perforated Baffles at Different Pitches, *Int. Comm. in Heat and Mass Transfer*, vol. 36, pp. 264-268, (2009).

[15] I. Ziolkowska, M. Dolata, D. Ziolkowski, Heat and Momentum Transfer in Fluids Heated in Tubes with Turbulence Generators at Moderate Prandtl and Reynolds Numbers. *Int. J. Heat Mass Transfer*, vol. 42, N° 4, pp. 613-627, (1999).

[16] Y. L. Tsay, J.C. Cheng and T. S. Chang, Enhancement of Heat Transfer from Surface-mounted Block Heat Sources in a Duct with Baffles, *Numerical Heat Transfer*, Part A, vol. 43, N° 8, pp. 827-841, (2003).

[17] Y. T. Yang, C. Z. Hwang, Calculation of Turbulent Flow and Heat Transfer in a Porous-baffled Channel. *Int. J. Heat Mass Transfer*, vol. 46, N° 5, pp. 771-780, (2003).

[18]M. Yilmaz, The effect of Inlet Flow Baffles on Heat Transfer, *Int. Comm. Heat Mass Transfer*, vol. 30, N° 8, pp. 1169-1178, (2003).
[19]S. Sripattanapipat and P. Promvonge, Numerical Analysis of Laminar Heat Transfer in a Channel with Diamond-Shaped Baffles, *Int. Comm. Heat Mass Transfer*, vol. 36, pp. 32-38, (2009).
[20]F. Wang, J. Zhang and S. Wang, Investigation on Flow and Heat Transfer Characteristics in Rectangular Channel with Drop-Shaped Pin Fins, *Propulsion and Power Research*, vol. 1, N° 1, pp. 64-70, (2012).
[21]N. Guerroudj and H. Kahalerras, Mixed Convection in a Channel Provided with Heated Porous Blocks of Various Shapes, *Energy Conversion Management*, vol. 51, pp. 505-517, (2010).
[22]H. Benzenine, R. Saim, S. Abboudi and O. Imine, Numerical Analysis of a Turbulent Flow in a Channel Provided with Transversal Waved Baffles, *Thermal Science*, vol. 17, N° 3, pp. 801-812, (2013).
[23]P. Sriromreun, C. Thianpong and P. Promvonge, Experimental and Numerical Study on Heat Transfer Enhancement in a Channel with Z-Shaped Baffles, *Int. Comm. Heat Mass Transfer*, vol. 39, pp. 945-952, (2012).
[24]Y. G. Lei, Y. L. He, R. Li and Y. F. Gao, Effects of Baffle Inclination Angle on Flow and Heat Transfer of a Heat Exchanger with Helical Baffles, *Chemical Engineering and Processing: Process Intensification*, vol. 47, pp. 2336-2345, (2008).
[25]C. Dong, Y. -P. Chen and J. -F. Wu, Flow and Heat Transfer Performances of Helical Baffle Heat Exchangers with Different Baffle Configurations, *Applied Thermal Engineering*, vol. 80, pp. 328-338, (2015).
[26]J. Wen, H. Yang, S. Wang, Y. Xue and X. Tong, Experimental Investigation on Performance Comparison for Shell-and-Tube Heat Exchangers with Different Baffles, *Int. J. Heat Mass Transfer*, vol. 84, pp. 990-997, (2015).
[27]P. Promvonge, Heat Transfer and Pressure Drop in a Channel with Multiple 60° V-baffles, *Int. Commun. Heat Mass Transfer*, vol. 37, pp. 835-840, (2010).
[28]P. Promvonge, Numerical Analysis of Laminar Flow Heat Transfer in Square Duct with V-shaped Baffles, *Chiangmai University Int. Conference* 2011, vol. 1, N° 1 pp. 83-92, (2010).
[29]P. Promvonge and S. Kwankaomeng, Periodic Laminar Flow and Heat Transfer in a Channel with 45° Staggered V-baffles, *Int. Comm. Heat Mass Transfer*, vol. 37, pp. 841-849, (2010).
[30]S. Tamna, S. Skullong, C. Thianpong and P. Promvonge, Heat Transfer Behaviors in a Solar Air Heater Channel with Multiple V-baffle Vortex Generators, *Solar Energy*, vol. 110, pp. 720-735, (2014).
[31]W.Jedsadaratanachai, S.Suwannapan andP. Promvonge, Numerical Study of Laminar Heat Transfer in Baffled Square Channel with Various Pitches, *Energy Procedia*, vol. 9, pp. 630-642, (2011).
[32]F. R. Menter, Two-equation Eddy-viscosity Turbulence Models for Engineering Applications, *J. AIAA.*, vol. 32, pp. 8, (1994).
[33]Fluent Inc., User´s Guide 6.3, Centerra Park Lebanon, NH, USA, 2006.
[34]S. V. Patankar, *Numerical heat transfer and fluid flow*, Hemisphere Publishing Corporation, New York, 1980.